

Recycled α -Fe₂O₃ nanoparticles adsorbents from Nd-Fe-B waste for methylene blue adsorption

M. Liu^a, Q.Y. Li^a, K. Gao^a, Y.J. Li^a, W.Q. Liu^a, Q.M. Lu^a, D.T. Zhang^a,
Z.S. Pang^b, X. Yu^b, C.H. Yu^b, S.S. Zha^c, Y.H. Liu^c, X.F. Yi^c, M. Yue^{a*}

^aLaboratory of Advanced Functional Materials, Ministry of Education, Faculty of Materials and Manufacturing, Beijing University of Technology, Beijing, 100124, China

^bGanzhou Fortune Electronic Co., Ltd., Ganzhou 341000, China

^cEarth-Panda Advanced Magnetic Materials Co.,Ltd., Hefei, 231500, China

Nanoparticles α -Fe₂O₃ were prepared using the waste liquid after recycling rare earths in Nd-Fe-B waste magnets. The most α -Fe₂O₃ particles have around 60-120nm diameters with the surface area of 144.51 m² g⁻¹ and pore size of around 5.0 nm. Methylene blue was used as a model pollutant to study the adsorption properties of the obtained α -Fe₂O₃ nanoparticles. The effects of contact time, pH value, loading mass of α -Fe₂O₃, and temperatures on the adsorption behavior were investigated. Results indicated that ultra-refined α -Fe₂O₃ particles can achieve an adsorption rate of 98% for the removal of methylene blue from waste liquids. Also, the removal of methylene blue by α -Fe₂O₃ particles presented an adsorption isotherm process which strongly fitted the pseudo-second-order kinetics model and Langmuir equation. The present work demonstrates a sustainable and efficient methodology for the re-use of Fe from magnet wastes and removal of MB, opening a promising and cost-effective avenue for the sewage-cleaning.

(Received May 26, 2021; Accepted September 24, 2021)

Keywords: Recycle, α -Fe₂O₃ nanoparticles, Nd-Fe-B, Methylene blue,
Adsorption mechanism

1. Introduction

Water is essential to the existence of life, economic development and societal progress [1]. The water damage caused by synthetic dyestuffs and heavy metal ions has nowadays become a global challenge because of the increasing awareness of environmental protection [2-4]. According to the data, more than 10⁴ tons of dyes are released into the environment each year [5]. Methylene blue (MB) is the hazardous organic dyes that exists in wastewater and becomes a threat to the water environmental safety and human health [6]. Therefore, it has attracted great interest to reduce the concentration of MB in wastewater.

* Corresponding author: magnetic@bjut.edu.cn

In recent study, nanostructured Fe_2O_3 with high specific surface area and accessible surface adsorption sites is used in the adsorption field, such as Fe_2O_3 nanorods [7], $\alpha\text{-Fe}_2\text{O}_3$ nanoellipsoids [8], $\gamma\text{-Fe}_2\text{O}_3/\text{SiO}_2$ composite [9], $\alpha\text{-Fe}_2\text{O}_3/\text{Cu}_2\text{O}$ composite [10] and magnetic $\alpha\text{-Fe}_2\text{O}_3$ /mesoporous silica nanocomposite [11]. Although the current researches have made some breakthroughs, most of production of adsorbents comes from pure iron sources. Considering the resources, environment and economy, it is more meaningful to find a low-cost way to produce Fe_2O_3 .

Neodymium-iron-boron (Nd-Fe-B) magnets as important parts in electroacoustic motors computers, mobile phones and smart electric devices, contain about 30wt. % of rare metals and 60wt. % Fe [12-15]. The growing demands from the rapid development of clean energy technology requires to increase the production of Nd-Fe-B by an anticipated 10% annual growth between 2020 and 2030 [16]. Nevertheless, the manufacturing and machining processes produce tremendous Nd-Fe-B magnet waste, which is 15% ~ 30% of the total production. If these Nd-Fe-B waste were not reasonably reused, it should cause a large money-loss, resource-waste, and environmental pollution [17]. Various strategies have been developed to recycle the rare earth elements through effective hydrometallurgy methods, such as selective precipitation [18] and co-precipitation [19], solvent extraction process [20] and ionic liquids extraction [21]. The reuse of Fe from the Nd-Fe-B waste, in contrast, has been overlooked for a long time and rarely reported due to its lower price and abundant resource. However, nonstandard disposal of Fe waste causes a permanent damage to the water environment and health problems, like cancer and genetic mutation, to living organisms [22-24]. Thereby, the re-use of the large amount of Fe via rational and cost-effective strategies is very important.

We herein put forward to a beneficial and flexible strategy to convert the remaining liquid after the recovery of rare earths from Nd-Fe-B wastes into $\alpha\text{-Fe}_2\text{O}_3$ nanoparticles for sewage treatment. MB was used as a model pollutant to study the adsorption properties of the obtained $\alpha\text{-Fe}_2\text{O}_3$ nanoparticles. The results show that it is an economic and environmental friendly method to convert the iron element in Nd-Fe-B waste into $\alpha\text{-Fe}_2\text{O}_3$ adsorbent.

2. Experimental Section

2.1. Synthesis of $\alpha\text{-Fe}_2\text{O}_3$ particles

At room temperature, the Nd-Fe-B waste was dissolved in HCl solution and oxalic acid was subsequently added into the leaching solution to separate the rare earth and Fe elements. The remaining iron ion liquid was used to raw material to prepare $\alpha\text{-Fe}_2\text{O}_3$ after depositing rare earth ions. 0.37g/L iron ion waste solution and 1.0g starch were dispersed in 10ml deionized water under stirring. The turbid sol mixture was aged for 15mins at 90°C by magnetic heated stirrer until the pasty gel particles obstruct rotor motion. After that, the rotor was separated with an external magnetic field and the pasty gel was heated for another 2-3mins to remove the remaining water. The obtained gel was dried by freeze drying method at -20°C for 48h. Finally, $\alpha\text{-Fe}_2\text{O}_3$ nanoparticles was obtained by calcining gel powder at 380°C for 6h in a quartz tube furnace.

2.2. Adsorption experiment

The adsorption of α -Fe₂O₃ on MB dyes was studied by batch experiments. An amount of α -Fe₂O₃ powder (0.040g-0.065g) was added to 100 mL MB with different initial concentrations (20mg/L-120mg/L). The initial pH (3.0-13.0) of solution was adjusted by using CH₃COOH/NaHCO₃ buffer and then the solution was subjected to stirring at 100r/min. Meanwhile, the experimental temperature (293-318K) and absorbed time (2-60mins) on adsorption reaction was discussed. At given time intervals, the 5ml solution containing MB was extracted for analyzing by a UV-vis spectrophotometer (Gem UV-100) at 665 nm, which is the maximum absorbance of MB. The adsorption capacity of MB was calculated according to the following equation:

$$q = \frac{(C_0 - C) * V_0}{m} \quad (1)$$

$$\eta = \frac{(C_0 - C) * 100\%}{C_0} \quad (2)$$

where q (mg/g) is the amount of adsorption, η is the adsorption capacity of MB, C_0 (mg/L) and C (mg/L) are the initial MB concentration and the equilibrium MB concentration, respectively. V_0 (mL) is the volume solution, and m (g) is the mass of the adsorbents.

2.3. Characterization of α -Fe₂O₃

The crystal structure was confirmed by X-ray Diffraction (XRD) on D8 Advance X-ray diffraction spectrometer (Bruker, German) with Cu K α radiation at 40 kV and 40 mA. Samples surface morphologies were observed by the scanning electron microscope (SEM, QUANTA FEG450, FEI, USA), transmission electron microscope (TEM, JEM-2011, JEOL, Japan) and high-resolution transmission electron microscopy (HRTEM). Fourier-transform infrared (FTIR) spectra were measured on a Tensor II series FT-IR spectrometer (Bruker, German). The specific surface area was calculated by the Brunauer-Emmett-Teller (BET) method on a specific surface area analyzer Micromeritics ASAP2020 (Micromeritics, USA).

3. Results and discussion

3.1. Characterization of α -Fe₂O₃

Fig. 1(a) shows the XRD diffraction pattern of the obtained α -Fe₂O₃ powder. These peaks at $2\theta = 33.12^\circ, 35.61^\circ, 40.85^\circ, 49.56^\circ, 54.11^\circ, 62.45^\circ$ and 63.96° correspond to (104), (110), (113), (024), (116), (214) and (300) lattice planes of body-centered cubic α -Fe₂O₃, respectively, which are consistent with the data of PDF no. 33-664 (α -Fe₂O₃). In addition, no impurity phase including rare earth is found in the XRD patterns, which indicates that iron ions are separated well from rare earth ions by oxalic acid deposition.

SEM image (Fig. 1(b)) indicates that the generated powder is made up of numerous nanoscale spheres. In process, the starch can build a gel system with a three-dimensional network carbon skeleton evenly filled with Fe(OH)₃ gel particles due to the interfacial energy and good synergies between iron and carbon atoms. Fe(OH)₃ particles were bound into of carbon skeleton with the sublimation of water at a low temperature and negative pressure during freeze drying.

When being calcined, carbon skeleton was oxidized into CO_2 and $\text{Fe}(\text{OH})_3$ was decomposed into Fe_2O_3 nanoparticles with good dispersity.

The specific surface area plays a vital role for the area of the adsorbed contact interfacial in the adsorption process. Generally, the adsorption capacity tends to increase with growth of specific surface area. The specific surface area and pore size distribution of the $\alpha\text{-Fe}_2\text{O}_3$ was confirmed by nitrogen adsorption-desorption experiments. As shown in Fig. 1(c), the nitrogen adsorption isotherm of $\alpha\text{-Fe}_2\text{O}_3$ exhibits a type IV curves with a hysteresis loop, which is one of the main characteristics of mesoporous materials. According to the international union of pure and applied chemistry classification, the hysteresis loop is ascribed to type H4 loops which is attributable to adsorption-desorption with narrow slit-like pores. The calculated the $\alpha\text{-Fe}_2\text{O}_3$ is $144.51 \text{ m}^2 \text{ g}^{-1}$ and most of the pore size distribution is around 5.0 nm.

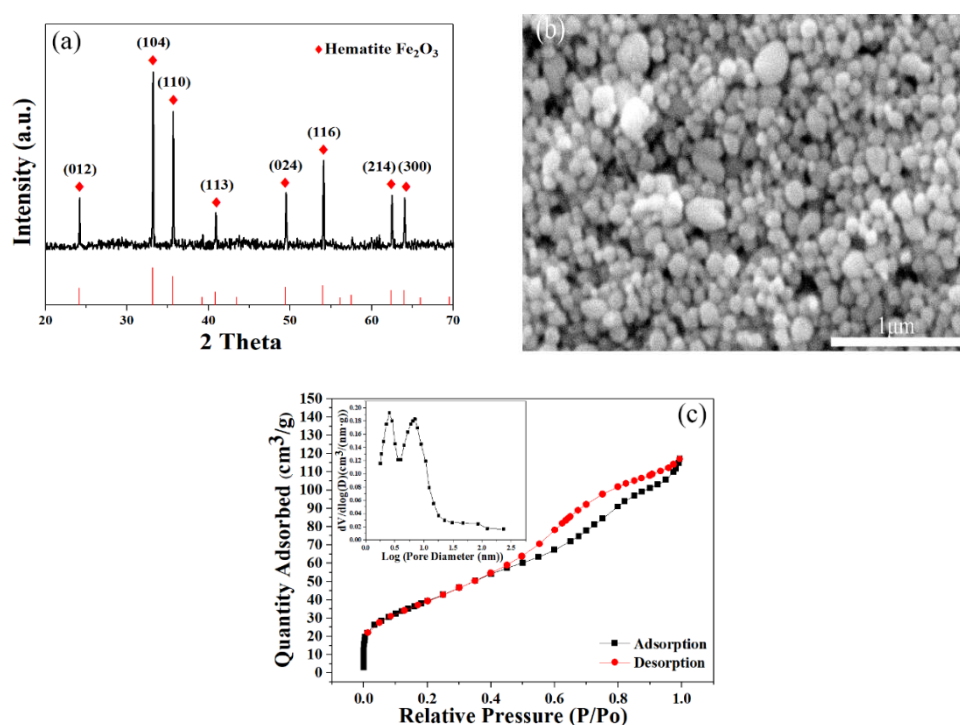


Fig. 1. (a) XRD pattern, (b) SEM image, (c) N_2 adsorption-desorption isotherms of $\alpha\text{-Fe}_2\text{O}_3$ nanospheres.

TEM image of the $\alpha\text{-Fe}_2\text{O}_3$ particles are shown in Fig. 2(a). The sample displays a uniform and homogenous spherical shape. The particles diameters are around 60-120nm and most of them are below 90nm. From the image Fig. 2(b) and Fig. 2(c), the distance between densely packed spheres is about 2-3nm which provides advantageous condition for the adsorption of dyes. The HRTEM (Fig. 2(c)) micrograph indicates that the intrinsic structure with lattice fringes of 0.37 and 0.25 nm, corresponds to the (012) and the (110) plane of $\alpha\text{-Fe}_2\text{O}_3$ crystal. The data obtained from the TEM and HRTEM are in excellent agreement with the SEM and XRD results. These results further indicate that the obtained $\alpha\text{-Fe}_2\text{O}_3$ can be expected as a promising adsorbent for the wastewater treatment due to its dimensional characteristics of nanoparticles.

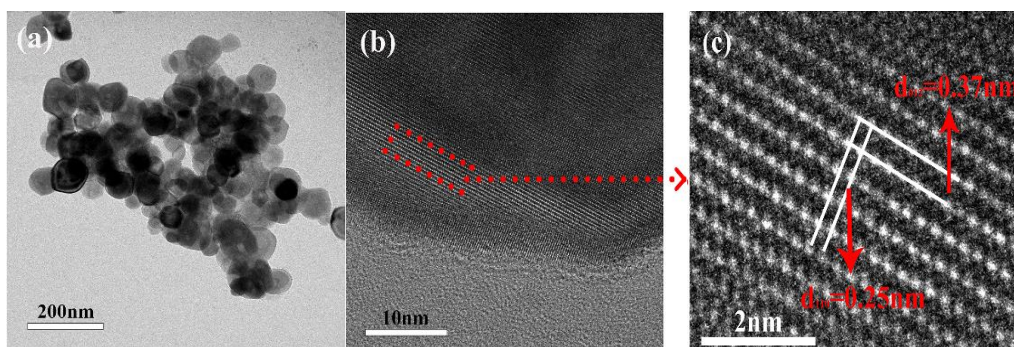


Fig. 2. (a) TEM, (b,c) HRTEM images of α - Fe_2O_3 .

3.2. Effect of various parameters on the MB adsorption

MB served as a model pollutant to evaluate the adsorption capacity of prepared α - Fe_2O_3 . As shown in Fig. 3(a), the adsorption process can be divided into three stages (i) the adsorption rate rapidly increases to 80.15% within first 5 min due to the large number of sites available for sorption; (ii) in 5-30min, the adsorption rate increases slowly and gradually stabilizes because the molecular mass transfer rate becomes slow and the number of accessible sites has dropped dramatically with the most MB molecular being absorbed; (iii) the last stages achieves the absorption equilibrium in 30-60min. The results perform that α - Fe_2O_3 particles have excellent adsorption characteristics to remove MB, with high adsorption speed and a removal efficiency of over 85%.

The pH values of a solution affect the dissociation of acidic or basic dyes [25]. The adsorption capacities at different pH values of initial solution are given in Fig. 3(b). The maximum of the adsorption capacity happens at pH 9.0. A part of active sites on the α - Fe_2O_3 surface are occupied by H^+ ions as pH values is lower, which leads to the reduction of active sites to absorb MB cationic. At the same time, co-action of electrostatic repulsion and steric hindrance of H^+ ions will also prevent MB cationic from being absorbed. So, the adsorption capacity decreases from 87% to 64% with the decrease of pH value from 9.0 to 3.0. However, parts of MB cationic easily combine with OH^- anions due to electrostatic attraction when pH values are higher. Therefore, the adsorption percent of MB decreases with increasing pH values from 9.0 to 13.0 because the MB failed to effectively compound with α - Fe_2O_3 . Finally, the maximum of the adsorption capacity happens at a proper pH value of 9.0 in our study.

In order to study MB mass adsorbed by α - Fe_2O_3 unit mass, different amounts of α - Fe_2O_3 (from 0.0400g to 0.0650g) were mixed with 100ml simulated sewage with MB initial concentration 40mg L^{-1} . Both the adsorption capacity and adsorbed MB mass increase with increasing adsorbent dosage from 0.0400g to 0.0550g (Fig. 3(c)). However, as further increment of adsorbent dosage above 0.0600 g, the adsorption capacity fails to bring a significant change, which means that α - Fe_2O_3 won't adsorb MB cationic when the MB concentration is lower than a certain value. The lowest MB concentration that α - Fe_2O_3 can adsorb MB cation is about 0.8 ppm in this study, which is basically harmless to water quality. So, although the adsorbent dosage keeps increasing, the adsorbed MB mass decreased evidently above the biggest adsorption capacity. It is found that there is a saturated MB mass adsorbed by α - Fe_2O_3 unit mass, indicating that adsorption and desorption are in equilibrium at the 0.0550 g adsorbent dosage.

There are two main effects of temperature on the adsorption process: (i) increasing the temperature is considered to increase the diffusion rate of adsorbate molecules in the adsorbent particles; (ii) the equilibrium capacity of a specific adsorbent varies with temperature. As shown in Fig. 3(d), a series of experiments were conducted at temperature range of 293-318K. The results present the adsorption process is an endothermic reaction in which both the adsorbed MB mass and equilibrium adsorption capacity display almost linear rise with temperature increasing. MB cations have a larger diffusion coefficient at higher temperature, which are easy to be adsorbed due to sufficient energy to interact with α -Fe₂O₃ surface active sites.

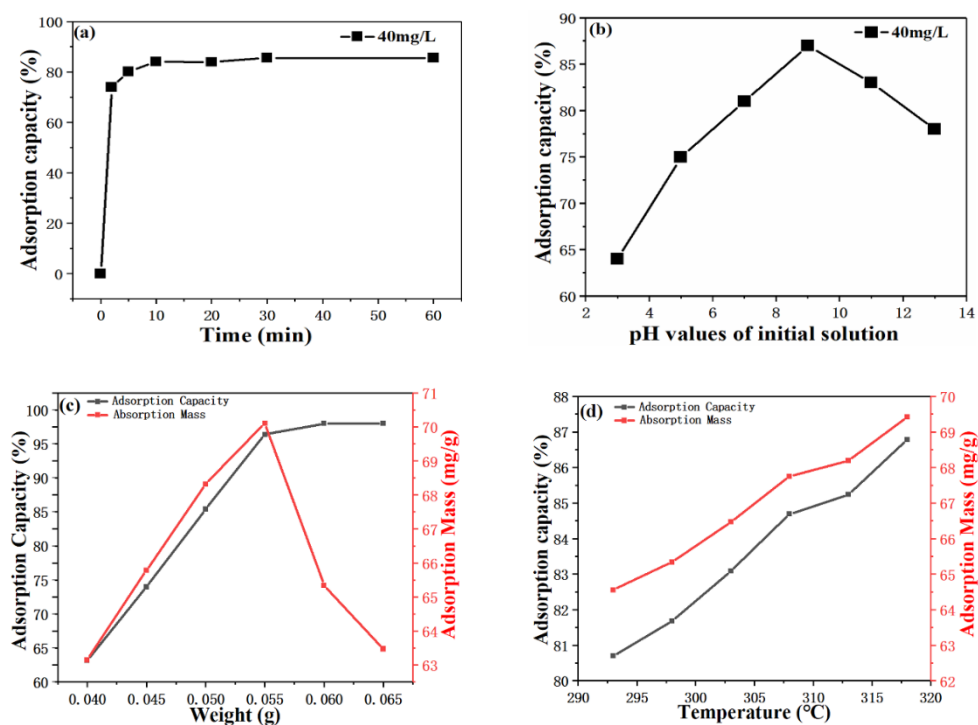


Fig. 3. Effect of (a) contact time, (b) pH values, (c) adsorption dosage and (d) temperature on MB adsorption by α -Fe₂O₃.

FTIR technique was used to judge the adsorption stability of α -Fe₂O₃ by testing the surface groups responsible for MB adsorption. Fig. 4(a) shows the FTIR spectra of α -Fe₂O₃ before and after adsorption. The characteristic adsorption peaks in wavenumber 456 cm⁻¹ and 553 cm⁻¹ of Fe-O bond reflect the existence of ferric oxide. Except for some slight differences in the 1000-1500 cm⁻¹ wavelength range, the position, number and intensity of absorption peaks before and after adsorption are almost the same, which indicates that the α -Fe₂O₃ particles have good adsorption stability. The infrared spectrum in a 1000-1700 cm⁻¹ range is amplified and that of MB was also added to carefully compare the differences between before and after adsorption. The peaks of MB can be detected in the spectra of α -Fe₂O₃ after adsorption, which confirms that MB has been successfully adsorbed on the surface of α -Fe₂O₃ while the α -Fe₂O₃ maintains the consistency of the electronic structure before and after adsorption.

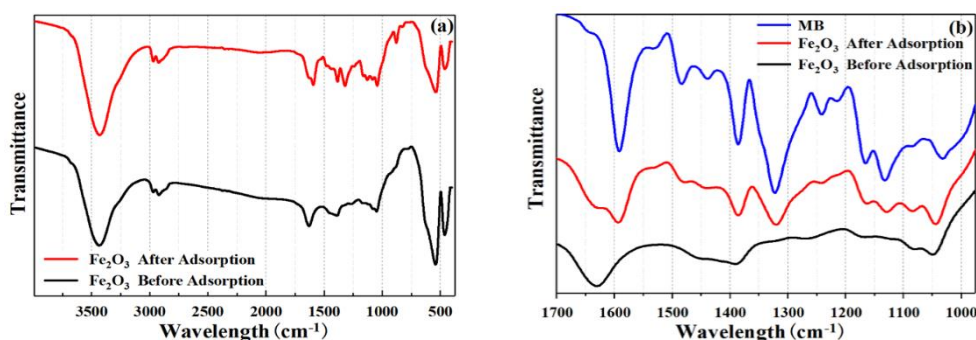


Fig. 4. FTIR spectra of α - Fe_2O_3 and MB.

3.3. Adsorption mechanism of the α - Fe_2O_3

The adsorption kinetics was mainly used to describe the adsorption efficiency and explore the mechanism of the adsorbent to optimize the adsorption performance [26]. In this study, to investigate the adsorption rate of α - Fe_2O_3 on MB, the pseudo-first-order Eq. (3) and pseudo-second-order models Eq. (4) [27,28] were evaluated according to the experimental data.

$$q_t = q_e(1 - e^{-K_1 t}) \quad (3)$$

$$q_t = \frac{K_2 q_e^2 t}{1 + K_2 q_e t} \quad (4)$$

where q_t (mg g^{-1}) and q_e (mg g^{-1}) are the concentrations of MB adsorbed at a given time t (min) and at equilibrium, respectively; K_1 (min^{-1}) is the rate constant of Eq. (3) for the adsorption, and K_2 ($\text{g mg}^{-1} \text{min}^{-1}$) is the rate constant of pseudo-second-order kinetic mode.

Table 1. Kinetics parameters of pseudo-first-order and pseudo-second-order model for α - Fe_2O_3 adsorption on MB

C_0 (mg L^{-1})	$q_{e,exp}$ (mg g^{-1})	Pseudo-first-order models			Pseudo-second-order models		
		$q_{e,cal}$ (mg g^{-1})	K_1 (min^{-1})	R^2	$q_{e,cal}$ (mg g^{-1})	K_2 ($\text{g mg}^{-1} \text{min}^{-1}$)	R^2
20	35.13	32.59	-1.064	0.9774	32.57	0.0788	0.9964
40	68.32	64.56	-1.029	0.9763	64.24	0.0226	0.9972
60	94.23	92.80	-0.9241	0.9619	91.38	0.0178	0.9940
80	126.10	123.99	-0.8851	0.9562	127.91	0.0165	0.9931
100	148.98	145.59	-0.6189	0.9541	146.53	0.0094	0.9861
120	174.86	170.88	-0.3718	0.9439	176.33	0.0079	0.9818

The corresponding adsorption rate constants were summarized in Table I. The evaluated equilibrium adsorption capacity $q_{e,cal}$ values were close to those $q_{e,exp}$ values from Eq. (4) but not from Eq. (3). What is more, the correlation coefficient (R^2) of pseudo-second-order model is much closer 1. Therefore, the adsorption kinetics data of α - Fe_2O_3 is accordance with the pseudo-second-order kinetics model. Applying simulation calculations to actual sewage treatment will quickly understand the rate of α - Fe_2O_3 adsorption of MB and the change trend of adsorption parameters, which can minimize the amount of α - Fe_2O_3 added to estimate the result and reduce the purification cost.

Adsorption isotherm refers to the nonlinear equation curve between the equilibrium adsorption capacity of solid adsorbate and the concentration of remaining liquid adsorbate. In

order to further realize and clarify and the adsorption mechanism, Langmuir Eq. (5) and Freundlich Eq. (6) isotherm models were used to fit experimental data. Langmuir isotherm can describe monolayer adsorption and the Freundlich isotherm model can be applied to non-ideal adsorption on heterogeneous surfaces as well as multilayer adsorption [29-31]. The Langmuir equation is

$$q_e = \frac{q_m b C_e}{1 + b C_e} \quad (5)$$

$$q_e = K_f C_e^{1/n} \quad (6)$$

where q_e (mg g^{-1}) is the adsorbed amount at equilibrium, q_m is the maximum adsorption capacity (mg g^{-1}) C_e is the equilibrium concentration (mg L^{-1}), b is adsorption constant of Langmuir (L mg^{-1}), K_f and n are the constants of Freundlich which refer to the relative adsorption capacity and process intensity, respectively.

Table 2 displays that the simulation results at 298, 308 and 318K with the same experimental details as above. Both the Freundlich equation and the Langmuir equation can match the adsorption process of $\alpha\text{-Fe}_2\text{O}_3$ within a certain range, but the Langmuir equation is more suitable for describing the adsorption behavior of MB on $\alpha\text{-Fe}_2\text{O}_3$.

Table 2. The parameters of Langmuir and Freundlich isotherms at different temperatures.

$T(K)$	Langmuir				Freundlich		
	$q_{m,exp}$ (mg g^{-1})	$q_{m,cal}$ (mg g^{-1})	b (L mg^{-1})	R^2	K_f	n	R^2
298	167.9	160.5	0.3068	0.9450	66.36	2.1938	0.8103
308	194.1	200.19	0.3833	0.9459	73.02	2.0561	0.8148
318	216.7	221.66	0.4909	0.9695	77.42	2.1756	0.8885

After fitting the Langmuir equation, the separation factor R_L Eq. (7) obtained under different indicates the adsorption process which is favorable ($0 < R_L < 1$) or unfavorable ($R_L > 1$) [32-33].

$$R_L = \frac{1}{1 + b C_0} \quad (7)$$

Table 3. Langmuir separation factor R_L of $\alpha\text{-Fe}_2\text{O}_3$ at a single temperature and different initial concentrations.

C_0 (mg L^{-1})	R_L		
	298K	308K	318K
40	0.0753	0.0612	0.0484
80	0.0342	0.0314	0.0287
120	0.0157	0.0145	0.0132

Table 3 shows R_L of $\alpha\text{-Fe}_2\text{O}_3$ are all between 0 and 1 which demonstrates the adsorption process of this type of adsorbent is preferential adsorption and has good adsorption capacity.

The thermodynamic parameters of $\alpha\text{-Fe}_2\text{O}_3$ adsorption process were obtained by

combining the Langmuir adsorption isotherm equation, Van't Hoof equation and thermodynamic equation [34-35]. The relationship is shown as the following Eq. (8) and Eq. (9).

$$\Delta G = -RT \ln K_c \quad (8)$$

$$\ln K_c = \frac{\Delta S}{R} - \frac{\Delta H}{RT} \quad (9)$$

where ΔG is Gibbs free energy (kJ mol^{-1}), K_c is the distribution coefficient of solute between adsorbent and solution in equilibrium (q_e / c_e , L g^{-1}). R is the gas constant ($8.314 \text{ J mol}^{-1} \text{ K}^{-1}$), T is the absolute temperature (K), ΔH and ΔS are enthalpy change (kJ mol^{-1}) and entropy change ($\text{kJ mol}^{-1} \text{ K}^{-1}$), respectively.

Table 4. The parameter of thermodynamics at different temperature.

$T(\text{K})$	$K_c(\text{L g}^{-1})$	ΔG (kJ mol ⁻¹)	ΔH (kJ mol ⁻¹)	ΔS (J mol ⁻¹ K ⁻¹)
298	6.102	-4.481	26	102.39
308	8.741	-5.551	26	102.39
318	12.463	-6.669	26	102.39

Table 4 described that all the values of ΔG were negative, which indicated that the adsorption process of MB on $\alpha\text{-Fe}_2\text{O}_3$ was spontaneous. Moreover, the ΔG of $\alpha\text{-Fe}_2\text{O}_3$ were between $-20\sim 0 \text{ kJ mol}^{-1}$, which proved that the process of this adsorption was physical adsorption. The ΔH values were positive, suggesting that the adsorption of MB on samples is an endothermic reaction process, which further verifies the inference above. The positive ΔS values indicated the reaction is an irreversible process.

4. Conclusion

Adsorptive nanoscale $\alpha\text{-Fe}_2\text{O}_3$ particles were prepared by sol-gel process using Fe recovered from Nd-Fe-B waste. The $\alpha\text{-Fe}_2\text{O}_3$ exhibits a uniform and homogenous spherical shape with specific surface area of the particles $144.51 \text{ m}^2 \text{ g}^{-1}$ and the pore size distribution 5.01 nm under the optimal preparation conditions of 1.0 g starch added and freeze drying. The absorption equilibrium achieved after 20 mins. The initial pH, adsorbent amount and reaction temperature on MB adsorption had significantly effects on the absorption reaction. These adsorption experiments have indicated that $\alpha\text{-Fe}_2\text{O}_3$ has excellent adsorption performance with high efficiency and good stability which are expected to become a promising adsorbent for the removal of MB from wastewater. The kinetic data of MB adsorption on $\alpha\text{-Fe}_2\text{O}_3$ fitted the pseudo-second-order kinetics model and Langmuir equation more closely matched the adsorption isotherm of the adsorption process. The calculated thermodynamic parameters indicated that adsorption was endothermic and spontaneous. Moreover, since the raw material comes from Nd-Fe-B waste which can reduce production costs and improve resource utilization, it proves the feasible idea of recovering iron from Nd-Fe-B waste.

Acknowledgments

This work is financially supported by the National Key Research and Development Program of China under Grant (2020YFC1909004), Science and technology program of Anhui Province (201903a07020002), the International Research Cooperation Seed Fund of Beijing University of Technology (No.2021B23) and National Key Research and Development Program of China (2019YFE0101900) and Program of Top Disciplines Construction in Beijing under Grant (PXM2019_014204_500031), China.

References

- [1] M. M. Gao, L. L. Zhu, C. K. Peh, G. W. Ho, *Energy Environ. Sci.* **12**(3), 841 (2019).
- [2] M. S. Chiou, H. Y. Li, *Chemosphere* **50**(8), 1095 (2003).
- [3] Z. Chen, H. Deng, C. Chen, Y. Yang, H. Xu, *Journal Of Environmental Health Science And Engineering* **12**(1), 63 (2014).
- [4] E.-K. Guechi, O. Hamdaoui, *Arabian Journal Of Chemistry* **9**, S416 (2016).
- [5] J. T. Harris, A. J. McNeil, *J. Polym. Sci.* **58** (21), 3042 (2020).
- [6] D. Wei, B. F. Wang, H. H. Ngo, W. S. Guo, F. Han, X. D. Wang, B. Du, Q. Wei, *Bioresour. Technol.* **185**, 14 (2015).
- [7] Q. Y. Chen, D. L. Huang, Y. B. Wang, J. Shao, L. L. Qu, *RSC Adv.* **6**(74), 70547 (2016).
- [8] A. Qurashi, Z. H. Zhong, M. W. Alam, *Solid State Sci.* **12**(8), 1516 (2010).
- [9] D. Chen, Z. Zeng, Y. Zeng, F. Zhang, M. Wang, *Water Resources and Industry* **15**, 1 (2016).
- [10] A. Norouzi, A. Nezamzadeh-Ejhih, *Physica B* **599**, 9 (2020).
- [11] I. Ursachi, A. Stancu, A. Vasile, *J. Colloid Interface Sci.* **377**, 184 (2012).
- [12] O. Gutfleisch, M. A. Willard, E. Bruck, C. H. Chen, S. G. Sankar, J. P. Liu, *Adv. Mater.* **23**(7), 821 (2011).
- [13] X. Y. Du, T. E. Graedel, *Sci. Total Environ.* **461**, 781 (2013).
- [14] N. Swain, S. Mishra, *J. Clean Prod.* **220**, 884 (2019).
- [15] A. Lukowiak, L. Zur, R. Tomala, T. N. LamTran, A. Bouajaj, W. Streck, G. C. Righini, M. Wickleder, M. Ferrari, *Ceram. Int.* **46** (16), 26247 (2020).
- [16] R. Schulze, M. Buchert, *Resour. Conserv. Recycl.* **113**, 12 (2016).
- [17] T. Horikawa, K. Miura, M. Itoh, K. Machida, *Journal Of Alloys And Compounds* **408**, 1386 (2006).
- [18] A. Kumari, M. K. Sinha, S. Pramanik, S. K. Sahu, *Waste Manage.* **75**, 486 (2018).
- [19] Y. Tian, Z. Liu, G. Zhang, *Journal of Rare Earths* **37**(2), 205 (2019).
- [20] E. Padhan, A. K. Nayak, K. Sarangi, *Hydrometallurgy* **174**, 210 (2017).
- [21] S. Riano, K. Binnemans, *Green Chem.* **17**(5), 2931 (2015).
- [22] Q. Y. Lv, X. S. Hu, X. L. Zhang, L. Y. Huang, Z. P. Liu, G. X. Sun, *Mater. Des.* **181**, 11 (2019).
- [23] Q. Y. Lv, X. S. Hu, Y. Shen, G. X. Sun, *J. Appl. Polym. Sci.* **437**, 33 (2020).
- [24] P.-J. He, Z. Xiao, L.-M. Shao, J.-Y. Yu, D.-J. Lee, *Journal Of Hazardous Materials* **137**(3), 1385 (2006).
- [25] M. Dogan, H. Abak, M. Alkan, *Journal Of Hazardous Materials* **164**(1), 172 (2009).

- [26] G. C. Chen, X. Q. Shan, Y. Q. Zhou, X. E. Shen, H. L. Huang, S. U. Khan, *Journal Of Hazardous Materials* **169**(1-3), 912 (2009).
- [27] J. W. Wang, W. K. Zhang, X. B. Zhang, F. M. Wang, Y. Q. Yang, G. J. Lv, *Journal Of Alloys And Compounds* **826**, 10 (2020).
- [28] Y. L. Zhang, G. Z. Ji, C. J. Li, X. X. Wang, A. M. Li, *Chem. Eng. J.* **390**, 11 (2020).
- [29] A. Nilchi, T. S. Dehaghan, S. R. Garmarodi, *Desalination* **321**, 67 (2013).
- [30] V. Ranjithkumar, S. Sangeetha, S. Vairam, *Journal Of Hazardous Materials* **273**, 127 (2014).
- [31] M. H. Tang, X. L. Huang, Y. Q. Peng, S. Y. Lu, *Fuel* **270**, 9 (2020).
- [32] P. Ding, K. L. Huang, G. Y. Li, Y. F. Liu, W. W. Zeng, *Int. J. Biol. Macromol.* **39** (4-5), 222 (2006).
- [33] Y. F. Ruan, B. Gao, *J. Mol. Struct.* **1210**, 10 (2020).
- [34] S. Y. Jia, D. Y. Tang, J. Peng, X. Yang, Z. J. Sun, *Chem. Eng. J.* **390**, 13 (2020).
- [35] H. A. Abbas, R. A. Nasr, A. Khalaf, A. Al Bawab, T. S. Jamil, *Ecotox. Environ. Safe.* **196**, 10 (2020).